Available online at www.sciencedirect.com
ScienceDirect
Acta Materialia 55 (2007) 5549–5557
Acta MATERIALIA
www.elsevier.com/locate/actamat

The $TiCl_3$ catalyst in $NaAlH_4$ for hydrogen storage induces grain refinement and impacts on hydrogen vacancy formation

S. Singh [a], S.W.H. Eijt [a], J. Huot [b], W.A. Kockelmann [c], M. Wagemaker [a], F.M. Mulder [a,*]

[a] *Fundamental Aspects of Materials and Energy, Department of Radiation, Radionuclides and Reactors, Faculty of Applied Sciences, Delft University of Technology, Delft, The Netherlands*
[b] *Université du Québec à Trois Rivières, Québec, Canada*
[c] *ISIS, Rutherford Appleton Laboratory, Chilton, Oxfordshire, UK*

Received 5 April 2007; received in revised form 5 June 2007; accepted 7 June 2007
Available online 9 August 2007

Abstract

$TiCl_3$ acts as an efficient catalyst for $NaAlH_4$ (sodium alanate), altering its hydrogen sorption kinetics and reversibility considerably. In order to clarify its role, we performed in situ neutron diffraction experiments on protonated catalysed and uncatalysed $NaAlH_4$. The phase transformations were monitored in the first two reaction steps during hydrogen release and in the second step during reloading. Our study for the first time provides clear indications that both Ti_xAl_{1-x} and NaCl formed act as grain refiner for Al and NaH, respectively, preventing particle growth. Particle sizes generally stay small upon desorption and reloading of $TiCl_3$ catalysed $NaAlH_4$, while significant particle growth is observed for uncatalysed $NaAlH_4$. The small crystallite sizes and observed hydrogen vacancy formation greatly facilitate the mass transfer during loading and unloading. This study underlines the importance of grain refining for achieving reversibility and faster kinetics of the hydrogen sorption processes, with a crucial double role played by the catalyst.

Keywords: Neutron diffraction; Nanocrystalline materials; Hydrogen storage; Phase transformations; Grain refining

1. Introduction

During the last decade, there has been growing interest in the development of lightweight metal hydrides capable of reversible hydrogen storage at low and medium temperatures. In a future sustainable energy economy, hydrogen may serve as a clean energy carrier, reducing (and eventually eliminating) carbon dioxide and other greenhouse emissions. A main challenge is to achieve safe and reliable hydrogen storage technologies that meet operating conditions, performance and cost requirements [1]. From a practical point of view, hydrogen should be stored with high hydrogen content at near-room temperature and at (or around) the standard operation pressure of 1 bar. Catalyst-doped $NaAlH_4$ (sodium alanate) is considered to be a promising hydrogen storage material because of its relatively large reversible hydrogen capacity (theoretically: 5.6 wt.%; practically: ~4.5 wt.%) and moderately low operating temperature (150 °C) [1–7]. The high hydrogen capacity of $NaAlH_4$ can be attained in two-step decomposition upon heating the material, involving the intermediate phase Na_3AlH_6 (sodium aluminium hexahydride), NaH (sodium hydride) and aluminium metal [2–7]:

$$NaAlH_4 \rightleftarrows 1/3Na_3AlH_6 + 2/3Al + H_2 \quad (1)$$

$$1/3Na_3AlH_6 \rightleftarrows NaH + 1/3Al + 1/2H_2 \quad (2)$$

Bogdanovic et al. showed that catalysing the reactions by Ti nanoparticles lowers the sorption temperatures and the reactions become largely reversible [2]. Their first, groundbreaking study [3] showed that $NaAlH_4$ samples doped with Ti-compounds ($TiCl_3$ and $Ti(OBu)_4$) begin to decompose at pragmatic rates at temperatures of about 100 °C, well below the melting point of the compound at

* Corresponding author. Tel.: +31 152784870.
E-mail address: f.m.mulder@tudelft.nl (F.M. Mulder).

1359-6454/$30.00
doi:10.1016/j.actamat.2007.06.028

about 180 °C. Since this discovery, considerable work has been done on improving the catalytic effects and understanding the role of the catalyst in $NaAlH_4$ [2–11].

The significance of the role of catalyst is well known [2–11], but the mechanism by which Ti enhances the cycling kinetics of hydrogen and reversibility of reactions (1) and (2) is still a big issue in the hydrogen storage field [11,12]. In fact, even the location of the Ti atoms remains unclear. It is indicated that Ti dwells on the surface of the material enabling dissociation of hydrogen molecules, substitutes for Na possibly facilitating the decomposition reactions, attracts a large number of H atoms [13–15] or induces increased hydrogen vacancy formation [16,17]. A number of different theories about the possible local environment of Ti have been suggested [18,19], but while the valence state of Ti was proven to be $Ti^{(0)}$ [18,19], a clear experimental and theoretical consensus is still under development.

A further essential aspect is that the reversibility of reactions (2) and (1) requires long-range migration of metal species. Small crystallite sizes therefore may clearly facilitate the through-solid mass transfer of H, Al and Na atoms, in the subsequent hydrogen absorption reactions to yield Na_3AlH_6 and $NaAlH_4$.

The aim of the study presented here is to better understand the role of Ti and Cl as a catalyst in the kinetics of hydrogen cycling in catalysed $NaAlH_4$, and to investigate the importance of both catalyst and nanoscale particle sizes in achieving reversibility. Therefore, we performed in situ neutron diffraction measurements on protonated catalysed $NaAlH_4$ in a comparison with uncatalysed $NaAlH_4$, and studied the phase transformations along with the reactions occurring during the hydrogen release and D_2 reloading. We report the importance of grain refinement – the phenomenon of keeping crystallite sizes small – in the rehydrogenation process of catalysed $NaAlH_4$, and show that $TiCl_3$ plays a (previously unanticipated) crucial role in this process.

Finally, the hydrogen site occupation was monitored to provide new insights into hydrogen migration through the mixed phase structures. In particular, quantitative information on hydrogen-vacancy formation and hydrogen–deuterium exchange was deduced from the neutron scattering data. Pronounced hydrogen vacancy formation was observed which can play a crucial role in the diffusion of H and possibly also of Al and Na through the particles during uptake and release of H.

2. Experimental

A catalysed sample was prepared by milling powders of protonated $NaAlH_4$ (sodium alanate) and 2 mol% $TiCl_3$ (titanium chloride) purity 99.9999% in a Spex 8000 apparatus for 15 min. Both the $NaAlH_4$ and $TiCl_3$ were obtained from Aldrich. Neutron and X-ray diffraction on the alanate showed only $NaAlH_4$ diffraction peaks. We used a high energy milling which ensures that 15 min is sufficient for a good distribution of the catalyst. Alanate was ball milled with a ball to powder ratio of 10:1 (30 g of balls:3 g of alanate). As a reference, an uncatalysed $NaAlH_4$ sample was prepared in the same manner without addition of $TiCl_3$. The size of the $NaAlH_4$ particles after ball milling was ~110 nm in both cases. For the in situ neutron diffraction measurements both samples were loaded into quartz tubes under argon atmosphere and subsequently connected to a gas-handling system.

The catalysed and uncatalysed samples were heated to pre-determined temperatures between 100 and 250 °C. A constant flow of hydrogen gas at a pressure of 1–2 bar was maintained during hydrogen desorption at 100 °C in the catalysed sample in order to work under realistic pressure conditions for future applications. In contrast, in the uncatalysed sample a sudden increase in the hydrogen release rate after onset of the first decomposition step did not allow the maintenance of a controlled hydrogen flow.

The samples were placed under deuterium (D_2) at pressure to investigate the reloading behavior. After the first dehydrogenation step a pressure of 10 bar at 100 °C was applied for the catalysed sample in order to observe if Na_3AlH_6 shows uptake of D by exchanging H and D or by filling vacancies in the structure. Upon subsequent full decomposition of Na_3AlH_6 into NaH, Al and H_2 after the second desorption step, the catalysed sample was reloaded again at 150 °C and 10 bar (equilibrium pressure being 5 bar). The full conversion of NaH, Al and D_2 into $Na_3Al(H,D)_6$ was followed by a second decomposition of $Na_3Al(H,D)_6$ into Na(H, D) and Al at 150 °C. Reloading the uncatalysed sample was attempted solely after completion of the second decomposition step at 150 °C and at 10 bar, since $NaAlH_4$ melted occurred during the first decomposition step.

Every 10 min during these procedures described above a neutron diffraction pattern was acquired using the general materials diffractometer (GEM) at the ISIS facility at the Rutherford Appleton Laboratory [20], amounting to a total of 89 patterns for the catalysed and 30 patterns for the uncatalysed sample. GEM combines an extraordinary neutron count rate with a very large Q range and a good resolution facilitating detailed in situ measurements. Due to the high signal to noise ratios it was possible to work with fully protonated materials, although these give a high diffraction background due to incoherently scattered neutrons. There are 7290 neutron detectors grouped into seven banks, each with a different range of accessible d-spacing. All diffraction patterns were fitted using Rietveld refinement using the General Structure Analysis System and the Sequentz program [21]. The different detector banks were fitted simultaneously, while phase fractions, lattice parameters, hydrogen site occupancies, temperature factors and line widths were allowed to vary freely. The particle sizes were calculated directly using the broadening of the fitted profile.

Further, as a reference, protonated $NaAlH_4$ (sodium alanate) was ball milled with 2 mol% Ti (titanium) metal powder in a Spex 8000 apparatus for 120 min. This longer milling time was needed because the Ti-metal powder is less brittle than $TiCl_3$, and resulted in $NaAlH_4$ particle sizes of

~50 nm after ball milling. The ex situ X-ray diffraction (XRD) was performed on the Ti-catalysed sample using a Bruker-AXS Type D5005 at the Cu Kα wavelength.

3. Results

In situ neutron diffraction measurements were carried out on uncatalysed and $TiCl_3$-catalysed $NaAlH_4$. The diffraction patterns for the uncatalysed and catalysed $NaAlH_4$ were obtained during both dehydriding and hydriding reactions. Figs. 1 and 2 show the evolution of the diffraction patterns for the respective samples as a function of time as colored plots after subtraction of the fitted incoherent background which results from the use of protonated samples.

In case of the reference uncatalysed sample, as expected, four different phases, namely $NaAlH_4$, Al, Na_3AlH_6 and NaH, were observed during the whole desorption process. The evolution of the phase fractions of these four phases is presented in Fig. 3 as a function of time, as obtained by the Rietveld analysis.

For this $NaAlH_4$ sample, a small amount of both Al (~8 mol%) and Na_3AlH_6 (~3 mol%) was already present directly after ball milling, as observed in the diffraction pattern obtained at room temperature. A small increase in the released hydrogen pressure to ~350 mbar was observed at 150 °C, indicating the onset of the first decomposition step. When the sample was heated further, a significant increase in the amounts of Al and Na_3AlH_6 was observed in the diffraction pattern with a corresponding release of hydrogen gas. Incoherent scattering of neutrons due to the presence of hydrogen (protons) contributes significantly to the background level of the diffraction patterns. Therefore, the detected decrease of the background levels during hydrogen desorption provided a further measure for the release of hydrogen. At 190 °C, all diffraction peaks associated with the $NaAlH_4$ phase abruptly disappeared due to the melting of $NaAlH_4$. In contrast, the diffraction peaks from Na_3AlH_6 and Al were still present. The second decomposition step commenced at 230 °C, where the NaH and Al phases start to grow at the expense of the Na_3AlH_6 phase, and complete transformation into NaH and Al was reached at 250 °C. A subsequent attempt to reload the sample with deuterium using a 10 bar pressure at a temperature of 150 °C, i.e. well above the equilibrium pressure of 5 bar, showed that the uncatalysed sample could not be reloaded

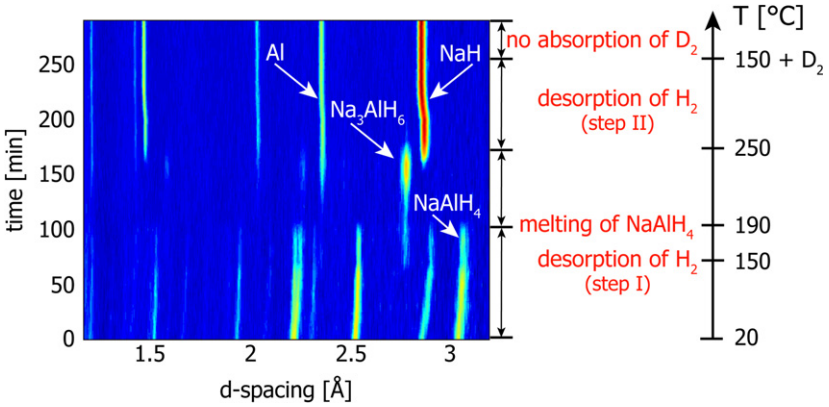

Fig. 1. Neutron diffraction patterns during desorption of hydrogen plotted against desorption time for uncatalysed $NaAlH_4$. The incoherent background was subtracted. The horizontal axis represents a small section of the *d*-spacing range measured. Bragg reflections of four different phases, $NaAlH_4$, Al, Na_3AlH_6 and NaH, are detected upon heating the uncatalysed sample.

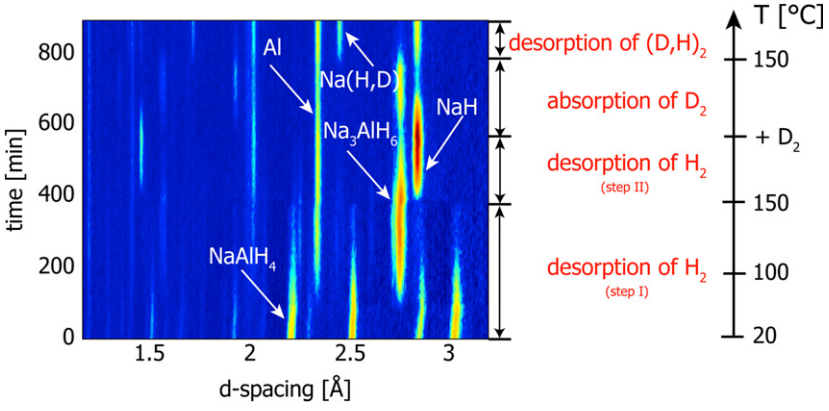

Fig. 2. Neutron diffraction patterns plotted against desorption time, showing the growth and decay of the different occurring phases, $NaAlH_4$, Al, Na_3AlH_6, NaCl and Na(H, D), during dehydriding and rehydriding of $TiCl_3$-catalysed $NaAlH_4$. The incoherent background was subtracted. The horizontal axis represents a small section of the total *d*-spacing range measured.

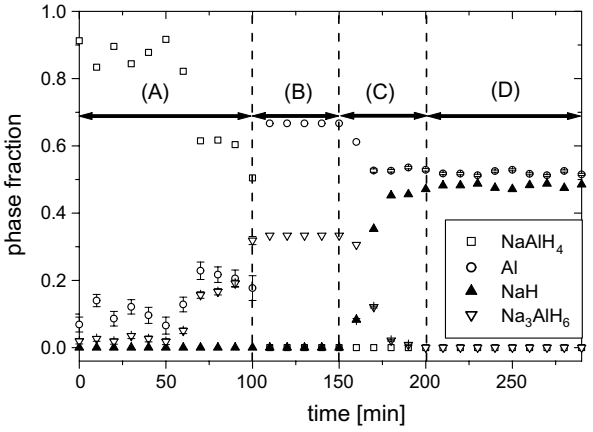

Fig. 3. Phase fractions of $NaAlH_4$ (□), Al (○), NaH (▲) and Na_3AlH_6 (▽) plotted over time during hydrogen desorption of uncatalysed $NaAlH_4$. The plot is divided into four time intervals, (A)–(D) representing: (A) desorption from room temperature to 190 °C; (B) melting and further desorption of $NaAlH_4$ at 190 °C and the presence of crystalline Al and Na_3AlH_6 (with an imposed fixed ratio of 2:1); (C) second step desorption in the temperature range of 230–250 °C; and (D) D_2 loading using a 10 bar pressure at 150 °C and subsequent further desorption.

reversibly. No peaks related to $Na_3Al(H,D)_6$ formation could be discerned in the diffraction patterns.

The evolution of the neutron diffraction patterns for the catalysed sample showed the presence of five different phases, namely $NaAlH_4$, Al, Na_3AlH_6, NaH and NaCl over time (see Fig. 4). Further, a complete reversibility of the second decomposition step was observed in this case in hydrogen cycling at 150 °C. In our study, no diffraction peaks were observed related to the presence of Ti, its hydride or alloys such as Ti_xAl_{1-x} or $TiCl_3$.

The first decomposition step was observed at 100 °C with a pressure of 1–2 bar and with a maintained H_2 flow. The $TiCl_3$-catalysed $NaAlH_4$ transformed completely into Na_3AlH_6 and Al in 270 min. There were no signs of NaCl

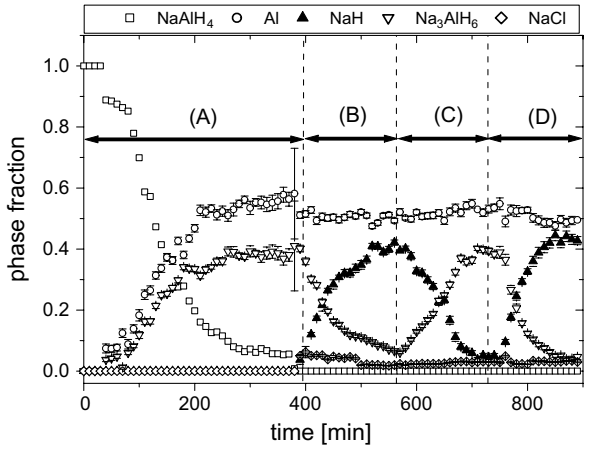

Fig. 4. Growth and decay of the $NaAlH_4$ (□), Al (○), NaH (▲), Na_3AlH_6 (▽) and NaCl (◇) phases given in terms of the extracted phase fractions in the $TiCl_3$-catalysed sample plotted against time. The plot is divided into four time intervals, (A)–(D) signifying: (A) first step desorption at 100 °C; (B) second step desorption at 150 °C; (C) 10 bar D_2 reloading at 150 °C; and (D) second step desorption at 150 °C.

formation during the first decomposition step. The second decomposition step started at 150 °C with formation of NaH and Al in a time interval of 150 min along with the observed desorption of hydrogen. In this case, NaCl was formed. Upon reloading the sample with deuterium using a pressure of 10 bar at 150 °C, the $Na_3Al(H,D)_6$ phase was formed successfully, resulting from the hydrogenation reaction involving NaH, Al and D_2. Subsequent desorption of $Na_3Al(H,D)_6$ resulted in the formation of Na(H, D) and additional Al.

The evolution of particle sizes was deduced from the broadening of the diffraction peaks using detailed Rietveld analysis. The dependence of the width of diffraction peaks on *d*-spacing is consistent with particle size-induced broadening and rules out significant strain broadening. The particle size of as-prepared ball-milled catalysed and uncatalysed $NaAlH_4$ obtained in this manner was ~110 nm for both samples. Upon desorption of the uncatalysed sample, no particle size broadening of the resulting NaH and Al was observed. Particle sizes are therefore estimated to be in the ~1 μm range (or larger), corresponding to the sensitivity limit of the backscattering bank of GEM for diffraction line broadening. For the catalysed sample, in

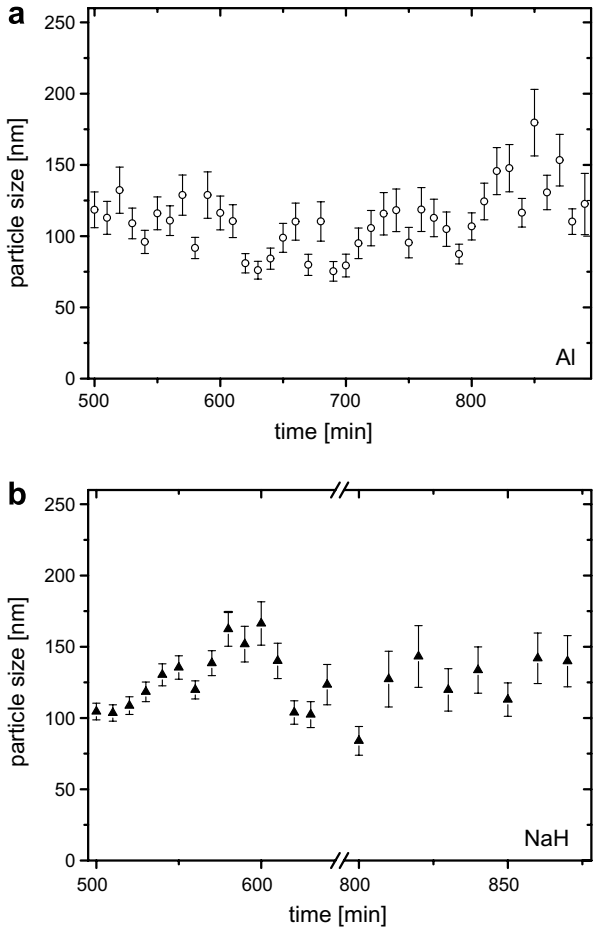

Fig. 5. Particle sizes of Al (a) and of NaH (b) over of time for the $TiCl_3$-catalysed $NaAlH_4$ sample, showing striking similarity in magnitude and a slight variation about an average size of ~120 nm.

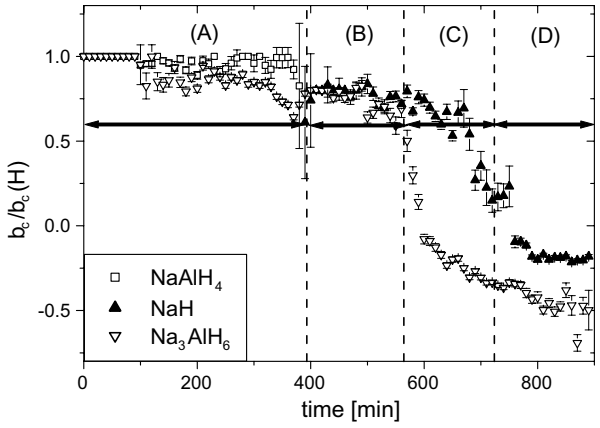

Fig. 6. Variation of the effective coherent scattering length b_c at the hydrogen sites normalized to b_c(H) for $NaAlH_4$, Na_3AlH_6 and NaH, respectively, over time for the $TiCl_3$-catalysed sample. In the time intervals (A) and (B), b_c/b_c(H) decreases due to hydrogen vacancy formation, while hydrogen–deuterium exchange leads to large reductions in the time intervals (C) and (D). The time intervals (A)–(D) represent: (A) first step desorption at 100 °C; (B) second step desorption at 150 °C; (C) 10 bar D_2 loading at 150 °C; and (D) pumping out of the D_2 and second step desorption at 150 °C.

contrast, the particle sizes of NaH and Al were only ~120 nm (i.e. small and also remarkably similar), with modest size changes during the various reactions (see Fig. 5). The particle sizes of NaCl and $Na_3Al(H,D)_6$ were found to be ~40 and ~200 nm, respectively.

A further important parameter is the evolution of the hydrogen site occupancy, determined by the Rietveld analysis of the neutron diffraction patterns. The extracted hydrogen site occupancy can vary either because of hydrogen vacancy formation or after D_2 exposure because of hydrogen–deuterium exchange since the coherent neutron scattering lengths of hydrogen and deuterium are very different and of opposite sign ($b_c(H) = -3.74$ fm and $b_c(D) = 6.67$ fm). In the uncatalysed sample, the hydrogen site remains fully occupied, staying stoichiometric for $NaAlH_4$, Na_3AlH_6 and NaH over time. On the other hand, a considerable change in the hydrogen site occupancy for Na_3AlH_6 and NaH was observed in the catalysed sample over time. Fig. 6 represents our results in terms of the observed effective scattering length b_c normalized to the scattering length of hydrogen $b_c(H) = -3.74$ fm for a fully occupied hydrogen site.

4. Discussion

4.1. Effect of particle sizes on hydrogen sorption properties

The neutron diffraction results clearly show that both the hydrogen desorption and the rehydrogenation behavior of the catalysed and uncatalysed samples is remarkably different. The hydrogen desorption in $TiCl_3$-catalysed $NaAlH_4$ evolves smoothly for both reaction steps (1) and (2) at a reaction timescale of the order of 150 min. The first reaction step in the uncatalysed $NaAlH_4$ sample, on the other hand, evolves only after abrupt hydrogen release and involves melting of the $NaAlH_4$ phase before complete transformation is reached. Further, reaction step (2) is reversible upon loading of D_2 (deuterium) for the catalysed sample under 10 bar at 150 °C. In contrast, it was observed that the uncatalysed sample could not be loaded reversibly using the same temperature and pressure conditions.

While the above phenomena were observed in earlier studies, a remarkable correlation between the particle sizes and the rehydrogenation reactions is observed here, which to our knowledge is not reported before in studies on $NaAlH_4$. Clearly, the sizes of the Al, Na_3AlH_6 and NaH particles for the uncatalysed sample grow significantly during the hydrogen release. In fact, the $NaAlH_4$ phase also showed growth of the particle size from 110 nm to ~280 nm when the temperature was raised to 160 °C (annealing) before the onset of the first decomposition step. On the other hand, particle sizes stay small even during cycling for the $TiCl_3$ catalysed sample. The latter showed successful loading of D_2 in the reaction step (2), and particle sizes of ~120 nm for NaH and Al were found. This clearly indicates that the particle size is an important factor in the rehydrogenation step. This can be easily understood since reversible hydrogen charging in these materials requires the transport of H, Al and Na ions, as well as mixing at the atomic level after phase separation has occurred. Clearly a small size of the crystallites reduces the required length scale of diffusion and will therefore enhance the kinetics of reloading [22–24]. In this respect, it should be noted that, for $NaAlH_4$ particles on a surface-oxidized carbon nanofiber support that have even smaller sizes of only a few nanometres, partial reversibility of the hydrogen sorption was also attained [25]. Here no transition metal catalyst was added, while the support is described as having no chemical reactions with the alanate during sorption or catalytic activity itself. When correct, this indicates the relevance of the diffusion length scale. Apart from this diffusion distance aspect, the small crystallite size also appears to induce significant vacancies in the hydrogen atomic lattice, as described in the following.

4.2. Hydrogen occupancy and vacancy formation

The role of hydrogen vacancies for hydrogen migration has been widely studied in interstitial metal hydrides. Together with diffusion along grain boundaries, vacancies have a large impact on the hydrogen sorption kinetics in crystalline solids. Nanoscopically small metal hydride particles may contain increased concentrations of defects [26], which may make hydrogen sorption reactions relatively fast. While recent debate on the role and presence of vacancies in $NaAlH_4$ and its decomposition compounds has focused on metal vacancies [27,28], here we show that significant hydrogen vacancy formation occurs for $TiCl_3$-doped $NaAlH_4$. Fig. 6 shows the development of the effective coherent hydrogen scattering lengths b_c for the $NaAlH_4$, Na_3AlH_6 and NaH phases over time for the

catalysed sample. A hydrogen vacancy concentration of about 20% is observed at the beginning of the Na_3AlH_6 phase formation in decomposition steps (1) and (2), respectively (time intervals A and B), determined from the decrease in effective scattering length. This reduction is deduced from the Rietveld analysis fitting, but is also directly observable in the changes in relative Bragg peak intensities for Na_3AlH_{6-x} in comparison with stoichiometric Na_3AlH_6 (see also Fig. 7). A similar H-vacancy density is observed for NaH in time interval B as deduced from the Rietveld analysis best fitting. Here, the changes are not easily deduced by the eye from the neutron diffraction patterns, since the intensities of the even index NaH_{1-x} Bragg peaks rise according to $I \sim |F_{hkl}|^2 \sim (b_c(\mathrm{Na}) + (1-x)b_c(H))^2 = (3.74x - 0.11)^2$ fm^2, or $I \sim (x - 0.03)^2$ for h, k, l even with hydrogen vacancy fraction x. Nevertheless, the Rietveld analysis fitting, in combination with the clearly observed H–D exchange discussed below, provide proof for the presence of increased hydrogen vacancy formation in NaH for the $TiCl_3$-catalysed $NaAlH_4$ sample.

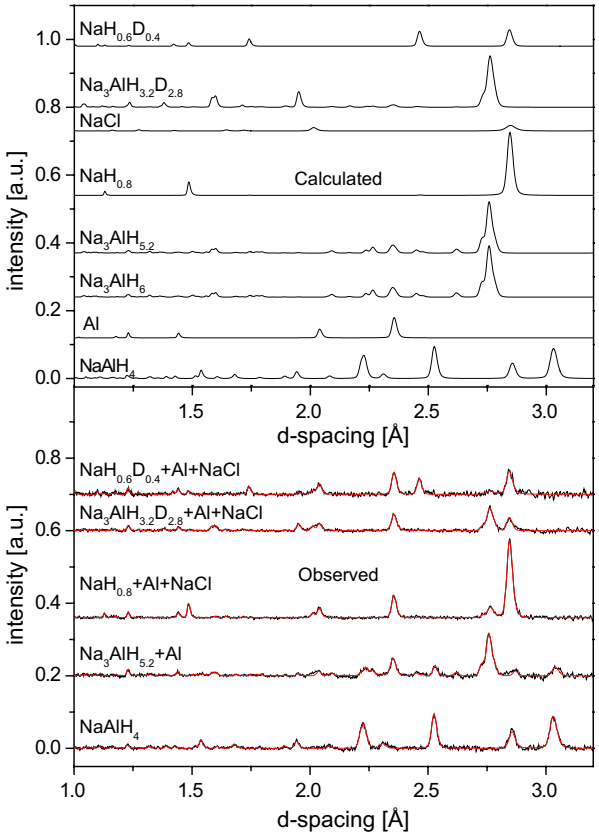

Fig. 7. Bottom: observed representative neutron diffraction patterns as a function of time for the $TiCl_3$-catalysed $NaAlH_4$ are shown together with Rietveld refinement, illustrating the effects of hydrogen vacancy formation in Na_3AlH_{6-x} and NaH_{1-x}, H–D exchange for Na(H,D) and incorporation of deuterium in the formed $Na_3Al(H,D)_6$ upon rehydrogenation. Spectra are plotted after the subtraction of the hydrogen incoherent background. Top: for clarity, simulated patterns extracted from Rietveld analysis are shown of the respective phases (bottom to top: $NaAlH_4$, Al, Na_3AlH_6, $Na_3AlH_{5.2}$, $NaH_{0.8}$, NaCl, $Na_3AlH_{3.2}D_{2.8}$, $NaH_{0.6}D_{0.4}$) separately. The simulated spectra for $Na_3AlH_{5.2}$ and $Na_3AlH_{3.2}D_{2.8}$ were normalized against the strongest peak of Na_3AlH_6 at a d-spacing of 2.755 Å.

The observed abundant unoccupied hydrogen sites may well facilitate hydrogen diffusion through the sample, as was reported previously by us in the case of nanostructured and catalysed MgH_{2-x} [26]. Hydrogen diffusion will only be appreciable in the case of a hydrogen-vacancy exchange mechanism because of the correspondingly low hydrogen migration energy. It may be stressed that the observed hydrogen occupancies for the $NaAlH_4$, Na_3AlH_6 and NaH phases in the case of the uncatalysed sample remain unchanged from the stoichiometric value of one, indicating negligible vacancy formation. The reason for vacancy formation in nanocrystalline (~120 nm) MgH_{2-x} in [26] was discussed in terms of the prevention of phase separation and its related strains and interfacial energy in nanoscale crystals. Similarly, strong structural changes were observed as a function of particle size in Li-insertion compounds with sizes between 7 and 120 nm that were analysed as the result of the prevention of intra-nanocrystallite phase separation [29]. Such effects related to phase separation may also occur here for the nanocrystalline reaction products of decomposition steps 1 and 2, promoting hydrogen vacancy formation. The increased vacancy formation in Na_3AlH_6 and NaH may furthermore be due to a reduction in the vacancy formation energy, either related to size effects (see above) or, in the case of Na_3AlH_6, to the presence of Ti, as suggested in recent ab initio studies on Na_3AlH_6 and $NaAlH_4$ [17] which showed that low hydrogen vacancy formation energies indeed can be reached. Palumbo et al. [16] recently showed the presence of local relaxation dynamics in the decomposition of $NaAlH_4$ samples using anelastic spectroscopy, indicating hydrogen vacancy formation in Na_3AlH_6. A mechanism for the vacancy formation was described based on the weakening of the local H–Al bonds, which they linked to the presence of Ti. A model was proposed to explain the increased hydrogen transport [16].

For hydrogen sorption in $NaAlH_4$, the situation is more complex than for nanocrystalline MgH_{2-x} because of the larger number of phases involved. Nevertheless, we propose that the large defect densities in the catalysed sample appear to be induced by the small scale of the NaH and Na_3AlH_6 crystallites, while also the Ti-catalyst may play a key role in the initial vacancy formation in Na_3AlH_6, as suggested by ab initio calculations and by anelastic spectroscopy studies. Ti is, however, not expected to play such a role for the NaH particles, since earlier TEM studies [30] demonstrated that for the NaH–Al state the Ti is entirely located in the Ti_xAl particles.

4.3. Grain refinement by the catalyst products NaCl and Ti_xAl_{1-x}

The impact of nanostructuring on the reversibility and (possibly together with the activity of Ti when incorporated in the Na_3AlH_6) on the hydrogen vacancies as recognized here will only last if the nanostructure is conserved after

the unloading and loading cycle. In studies on the solidification of liquid aluminium [31,32], it has been shown that $TiAl_3$ acts as a grain refiner for Al crystallites. Small $TiAl_3$ crystallites enhance the nucleation of solid aluminium. By their presence in sufficiently large quantities as dispersed nucleation centres they keep the Al grains small [31,32]. On the other hand, in the absence of sufficient nucleation centres superheating [33] may occur before structural phase transitions take place, yielding relatively few large Al crystallites. The uncatalysed $NaAlH_4$ could be heated even above its standard melting temperature of 180 °C, before major decomposition and melting, resulting in large $NaAlH_4$ and Al crystallites.

Previous synchrotron X-ray and XAFS studies on $TiCl_3$-doped $NaAlH_4$ clearly showed the presence of Ti_xAl_{1-x} alloys after cycling for 6–10 mol% $TiCl_3$ doping [19,34,35]. A TEM study on $NaAlH_4$ doped with 4 mol% $TiCl_3$ revealed the formation of $TiAl_3$ with hydrogen desorption [30]. We expect that Ti_xAl_{1-x} formation, therefore, also occurred in our experiment, but such Ti_xAl_{1-x} was not detected in the diffraction patterns possibly because of the small catalyst content and the overlap with the Al metal Bragg peaks. However, in view of the known grain refiner effect for $TiAl_3$ in Al alloys, it appears clear that Ti_xAl_{1-x} is also present here and prevents agglomeration of Al in large crystallites.

It is interesting to note that NaH and NaCl share the same (rock salt) crystallographic structure although there is a mismatch in unit cell size (~15%), see Table 1. This may facilitate NaCl to act as a grain refiner for NaH and vice versa. (In the second decomposition step, NaCl was shown to appear side by side with the NaH formation.) After NaCl has formed as ~40 nm small NaCl crystallites (size from diffraction line width), it may act as grain refiner for Na(H, D) in the last decomposition. Such a mechanism would facilitate stabilization of NaH particle sizes, as observed for the catalysed sample. Based on the sizes and concentrations, it is estimated that ~1–2 NaCl particles per NaH particle are formed, which seems adequate to provide nucleation centres and prevent NaH agglomeration. Interestingly, the presence of ~120 nm small NaH and Al particles for $TiCl_3$-doped $NaAlH_4$ seems optimum in this respect. Further, the observed size of the resulting Na_3AlH_6 crystallites (~200 nm on the average) matches well with the combined volume of 3 NaH and 1 Al crystallite of ~120 nm each.

4.4. Comparison with ex situ X-ray diffraction on Ti metal catalysed $NaAlH_4$

Haiduc et al. showed that doping of $NaAlH_4$ with either $TiCl_3$ or $Ti(OBu)_4$ results in the formation of different Ti-compounds upon hydrogen desorption [36]. For this reason, we studied the development of particle sizes by X-ray diffraction upon desorption of a 2 mol% Ti metal catalysed $NaAlH_4$ sample, enabling a comparison with $TiCl_3$-catalysed $NaAlH_4$. Clearly, the grain refiner action may well depend on the amount, type and structure of the Ti alloys formed. In contrast to the case of $TiCl_3$-catalysed $NaAlH_4$, the sizes of Al and NaH particles formed in the decomposition of $NaAlH_4$ and Na_3AlH_6 became a factor of 4, respectively 2 larger compared with the initial particle size of $NaAlH_4$ after ball milling (Table 2). The observed growth may indicate two factors: first, the disper-

Table 1
Obtained structural parameters of the phases observed during deuterium cycling of $TiCl_3$-catalysed ball milled $NaAlH_4$

$NaAlH_4$	
Lattice parameter at 100 °C	$a, b = 5.044$ Å, $c = 11.434$ Å
Space group	I 41/*a*
Atom site in Wyckoff notation	Na: 4*a* (0, 0.2500, 0.1250)
	Al: 4*b* (0, 0.2500, 0.6250)
	H: 16*f* (0.2340, 0.3860, 0.5500)
Occupancy	Na: 1.000, Al: 1.000, H: 1.000
Al	
Lattice parameter at 100 °C	$a, b, c = 4.064$ Å,
Space group	F *m*–3*m*
Atom site in Wyckoff notation	Al: 4*a* (0, 0, 0)
Occupancy	Al: 1.000
NaH	
Lattice parameter at 150 °C	$a, b, c = 4.91$ Å,
Space group	F *m*–3*m*
Atom site in Wyckoff notation	Na: 4*a*(0, 0, 0) H: 4*b* (0.5, 0.5, 0.5)
Occupancy	Na: 1.000
	H: 1.000 down to 0.72
Na_3AlH_6	
Lattice parameter at 100 °C	$a = 5.449$ Å, $b = 5.536$ Å, $c = 7.802$ Å
Space group	P 21/*n*
Atom site in Wyckoff notation	Na1: 2*a* (0, 0, 0.5)
	Na2: 2*b* (−0.006, 0.4601, 0.2518)
	Al: 4*e* (0, 0, 0)
	H1: 4*e* (0.091, 0.041, 0.215)
	H2: 4*e* (0.234, 0.328, 0.544)
	H3: 4*e* (0.165, 0.266, 0.944)
Occupancy	Na1: 1.000, Na2: 1.000, Al: 1.000
	H1, H2, H3: 1.000 down to 0.82
NaCl	
Lattice parameter at 150 °C	$a, b, c = 5.673$ Å
Space group	F *m*–3*m*
Atom site in Wyckoff notation	Na: 4*a* (0, 0, 0)
	Cl: 4*b* (0.5, 0.5, 0.5)
Occupancy	Na: 1.000, Cl: 1.000

Table 2
Comparison of the particle sizes of the $NaAlH_4$, NaH and Al phases during hydrogen sorption reactions in $TiCl_3$-catalysed and Ti-catalysed $NaAlH_4$

Sample	Sample treatment	Particle size (nm)		
		$NaAlH_4$	NaH	Al
$TiCl_3$-catalysed $NaAlH_4$	As prepared	110		
	150 °C, 150 °C + D_2, 150 °C *		120	120
Ti-catalysed $NaAlH_4$	As prepared	50		
	0.5 h at 150 °C		100	220
	2 h at 170 °C		120	220
	8 h at 180 °C		100	190

* See Fig. 5.

sion of Ti in the Ti_xAl_{1-x} may be different relative to $TiCl_3$-catalysed $NaAlH_4$, where the $TiCl_3$ catalyst may be dispersed more homogeneously, resulting in smaller Al crystallites. Second, the NaH phase grows a factor 2 compared with the initial particle size, providing a further indication that the mechanism proposed above where NaCl does indeed act as grain refiner. Without the presence of NaCl particles, the NaH particles show clear growth, whereas in the presence of NaCl the NaH particle sizes remain fixed to the size of the initial $NaAlH_4$ particles. An interesting observation (Table 2) is that with heating the sample during the second decomposition step at higher temperatures over prolonged times the NaH particles do not show any further growth. This may indicate that the presence of nanoscale Al crystallites, stabilized by Ti_xAl_{1-x} alloys, imposes a morphology in which the NaH particles cannot grow larger upon annealing.

4.5. Hydrogen–deuterium exchange in NaH during rehydrogenation

The development of the effective scattering lengths $b_c/b_c(H)$ of the Na_3AlH_6 and NaH phases (Fig. 6) both show a further significant reduction in time intervals C and D which correspond to D_2 loading of the mainly NaH and Al containing sample, and subsequent desorption of the formed $Na_3Al(H,D)_6$, respectively. The reduction of $b_c/b_c(H)$ is here primarily related to hydrogen–deuterium exchange processes [37] which become possible when deuterium pressure was applied to reload of the sample, and is not related to induced higher H vacancy densities. The observed negative values of $b_c/b_c(H)$ are caused by the opposite sign in the scattering length for D with respect to $b_c(H)$. Interestingly, the H–D exchange in NaH is clearly visible by the appearance of additional (even index) Bragg peaks in the neutron diffraction patterns, as shown in Fig. 7. The comparison of patterns before deuterium exchange with the pattern of the $NaH_{\sim 0.6}D_{\sim 0.4}$ composition finally reached in time interval D at $t = 890$ min shows that a complete set of Bragg reflections appear upon incorporation of deuterium. These peaks correspond to (hkl) reflections with even indices, while the NaH diffraction pattern only exhibits odd-index reflections (see Fig. 7). This is caused by accidental extinction of the even-index reflections because the coherent neutron scattering lengths of Na (3.62 fm) and H (−3.74 fm) are almost equal but of opposite sign. Therefore, the incorporated deuterium fraction x in $NaH_{1-x}D_x$ can be sensitively monitored by the rise of the even-index peaks in the neutron diffraction patterns, which increase according to $I \sim |F_{hkl}|^2 \sim (b_c(Na) + (1-x)b_c(H) + xb_c(D))^2 = (10.41x - 0.11)^2\ \mathrm{fm}^2$, or $I \sim (x - 0.01)^2$ for h, k, l even, upon hydrogen–deuterium exchange.

While D absorbed in the formed $Na_3Al(H,D)_6$ is clearly expected during deuterium loading in time interval C, the observed and simultaneously occurring H–D exchange in NaH is somewhat surprising. NaH is known to be a rather stable compound, with a very low hydrogen equilibrium pressure of about 0.01 mbar at 150 °C [38]. This infers that, despite the stability of NaH, H–D exchange happens fairly rapid for such NaH nanoparticles. Clearly, the presence of abundant hydrogen vacancy concentrations, as detected here, is essential for H–D exchange to occur on the observed timescale of ~100 min, because of the resulting correspondingly lower hydrogen migration energy. Further, this might suggest that the NaH particles play a role in dissociating hydrogen molecules at their surfaces [39]. More detailed forthcoming studies are needed to clarify this latter point.

In contrast, the neutron diffraction patterns of the uncatalysed sample showed no exchange of H–D since Bragg peaks characteristic for Na(H, D) formation remained absent throughout the complete desorption experiment and D_2 pressure application. In view of the above discussion, a plausible reason for absence of H–D exchange in the uncatalysed sample can thus be found in the large NaH particle sizes in which H vacancies are absent.

5. Conclusions

$TiCl_3$ catalysed and nanostructured $NaAlH_4$ has superior reversible hydrogen sorption characteristics compared with uncatalysed and nanostructured $NaAlH_4$. This study focused on understanding the evolution of the phases, morphology and hydrogen site occupancies during hydrogen release and D_2 absorption. Clear differences in these properties are observed comparing $TiCl_3$-catalysed $NaAlH_4$ with uncatalysed $NaAlH_4$ studied as a reference. Our results show for the first time that the reaction products $TiAl_x$ and NaCl induce grain refinement, maintaining the small particle sizes for the decomposition products, which plays an important role in the reversible hydrogen sorption characteristics. The $TiCl_3$ catalysed sample shows gradual phase transformations and approximately constant nanoscopic particle sizes throughout the hydrogen unloading and reloading reactions. In contrast, the initially nanostructured but uncatalysed material only decomposes after melting, and the resulting (micron range) large crystallites could not be reloaded. Effective grain refining action by the $TiAl_3$ and NaCl compounds, emerging naturally in the decomposition of the $TiCl_3$-catalysed sample only, is proposed as the explanation of this strikingly different morphology evolution for the catalysed sample.

The nanostructured and $TiCl_3$-catalysed sample reveals pronounced hydrogen vacancy formation in the resulting Na_3AlH_{6-x} and NaH_{1-x} phases, which will be of direct significance for the through-solid H diffusion, but possibly also for the mass transport of Al and Na required for reversibility. Such significant vacancy densities and chemical composition changes have recently also been observed in nanoscale MgH_x [26] and Li_xTiO_2 [29]. Furthermore, clear and relatively fast H–D exchange is observed in the nanoscale NaH_{1-x} phase of the catalysed sample when

D_2 pressure was applied, enabled by the hydrogen vacancies present. This further might suggest that these particles play a role in the dissociation of hydrogen molecules. Such exchange is absent in the large crystallites of the uncatalysed sample.

The achieved reversibility for $NaAlH_4$ is usually ascribed to the role of Ti incorporated in the (surface of) different crystallographic phases solely. This study reveals that the $TiCl_3$ has a further important role. The presence of $TiAl_x$ and NaCl induces maintained nanoscopic particle sizes, high H vacancy densities and H–D exchange in the catalysed sample. These clearly will also play a very significant role in the (complex) mechanism of reversible hydrogen sorption of $TiCl_3$ catalysed $NaAlH_4$.

Acknowledgements

This work was financed by the Sustainable Hydrogen Programme of the Delft Institute for Sustainable Energy (DISE), Delft University of Technology. W.J. Legerstee is acknowledged for support in the hydrogen desorption and X-ray diffraction analysis of Ti-catalysed $NaAlH_4$. Financial support was received from the Netherlands Organization for Scientific Research (NWO) for access to ISIS.

Appendix A. Supplementary material

Supplementary data associated with this article can be found, in the online version, at doi:10.1016/j.actamat.2007.06.028.

References

[1] Schlapbach L, Züttel A. Nature 2001;414:353.
[2] Bogdanovic B, Felderhoff M, Kaskel S, Pommerin A, Schlichte K, Schüth F. Adv Mater 2003;15:1012.
[3] Bogdanovic B, Schwickardi M. J Alloy Compd 1997;253–254:1.
[4] Bogdanovic B, Brand RA, Marjanovic A, Schwickardi M, Tolle J. J Alloy Compd 2000;302:36.
[5] Jensen CM, Gross KJ. Appl Phys A 2001;72:213.
[6] Gross KJ, Guthrie S, Takara S, Thomas GJ. J Alloy Compd 2000;297:270.
[7] Sandrock G, Gross KJ, Thomas GJ, Jensen CM, Meeker D, Takara S. J Alloy Compd 2002;330:696.
[8] Streukens G, Bogdanovic B, Felderhoff M, Schüth F. Phys Chem Chem Phys 2006;8(24):2889.
[9] Bogdanovic B, Felderhoff M, Pommerin A, Schüth F, Spielkamp N. Adv Mater 2006;18(9):1198.
[10] Bellosta von Colbe JM, Felderhoff M, Bogdanovic B, Schüth F, Weidenthaler C. Chem Commun 2005(37):4732.
[11] Gross KJ, Thomas GJ, Jensen CM. J Alloy Compd 2002;330–332:683.
[12] Kiyobayashi T, Srinivasan SS, Sun D, Jensen CM. J Phys Chem A 2003;107:7671.
[13] Thomas GJ, Gross KJ, Yang NYC, Jensen CM. J Alloy Compd 2002;330–332:702.
[14] Sun D, Kiyobayashi T, Takeshita HT, Kuriyama N, Jensen CM. J Alloy Compd 2002;337:L8.
[15] Iniguez J, Yildirim T. Appl Phys Lett 2005;86:103109.
[16] Palumbo O, Paolone A, Cantelli R, Jensen CM, Sulic M. J Phys Chem B 2006;110:9105.
[17] Peles A, Van de Walle CG. J Alloy Compd 2007. doi:10.1016/j.jallcom.2006.12.110.
[18] Leon A, Kircher O, Rothe J, Fichtner M. J Phys Chem B 2004;108:16372.
[19] Graetz J, Reilly JJ, Johnson J, Ignatov AY, Tyson TA. Appl Phys Lett 2004;85(3):500.
[20] Williams WG, Ibberson RM, Day P, Enderby JE. Physica B 1998;241–243:234.
[21] Larson AC, Dreele RBV. General Structure Analysis System (GSAS), LAUR 86-748, Los Alamos National Laboratory, 1994. Blake G. Sequentz program for sequential refinement using GSAS, ISIS facility 2004 Annual Report.
[22] Gross KJ, Spatz P, Züttel A, Schlapbach L. J Alloy Compd 1996;240:206.
[23] Huot J, Liang G, Boily S, Van Neste A, Schulz R. J Alloy Compd 1999;293–295:495.
[24] Bogdanovic B, Spliethoff B. Int J Hydrogen Energy 1987;12:863.
[25] Baldé CP, Hereijgers BPC, Bitter JH, de Jong KP. Angew Chem Int Ed 2006;45:3501.
[26] Schimmel HG, Huot J, Chapon LC, Tichelaar FD, Mulder FM. J Am Chem Soc 2005;127:14348.
[27] Araújo CM, Li S, Ahuja R, Jena P. Phys Rev B 2005;72:165101.
[28] Li S, Jena P, Ahuja R. Phys Rev B 2006;73:214107.
[29] Wagemaker M, Borghols WJH, Mulder FM. J Am Chem Soc 2007;129:4323.
[30] Weidenthaler C, Pommerin A, Felderhoff M, Bogdanovic B, Schüth F. Phys Chem Chem Phys 2003;5:5149.
[31] Iqbal N, Van Dijk NH, Hansen T, Katgerman L, Kearley GJ. Mater Sci Eng A 2004;386:20.
[32] Iqbal N, Van Dijk NH, Offerman SE, Moret MP, Katgerman L, Kearley GJ. Acta Mater 2005;53:2875.
[33] Belonoshko AB, Skorodumova NV, Rosengren A, Johansson B. Phys Rev B 2006;73:012201.
[34] Brinks HW, Jensen CM, Srinivasan SS, Hauback BC, Blanchard D, Murphy K. J Alloy Compd 2004;376:215.
[35] Brinks HW, Sulic M, Jensen CM, Hauback BC. J Phys Chem B 2006;110:2740.
[36] Haiduc AG, Stil HA, Schwarz MA, Paulus P, Geerlings JJC. J Alloy Compd 2005;393:252.
[37] Bellosta von Colbe JM, Schmidt W, Felderhoff M, Bogdanovic B, Schüth F. Angew Chem Int Ed 2006;45:3663.
[38] Sandrock G. J Alloy Compd 1999;293–295:877.
[39] Chaudhuri S, Muckerman JT. J Phys Chem B 2005;109:6952.